J. Fluid Mech. (2012), *vol.* 705, *pp.* 195–212.
doi:10.1017/jfm.2012.102

Motion of red blood cells near microvessel walls: effects of a porous wall layer

Daniel S. Hariprasad[1] **and Timothy W. Secomb**[2]†

[1] Program in Applied Mathematics, University of Arizona, Tucson, AZ 85721, USA
[2] Department of Physiology, University of Arizona, Tucson, AZ 85724, USA

(Received 19 July 2011; revised 31 January 2012; accepted 20 February 2012;
first published online 12 April 2012)

A two-dimensional model is used to simulate the motion and deformation of a single mammalian red blood cell (RBC) flowing close to the wall of a microvessel, taking into account the effects of a porous endothelial surface layer (ESL) lining the vessel wall. Migration of RBCs away from the wall leads to the formation of a cell-depleted layer near the wall, which has a large effect on the resistance to blood flow in microvessels. The objective is to examine the mechanical factors causing this migration, including the effects of the ESL. The vessel is represented as a straight parallel-sided channel. The RBC is represented as a set of interconnected viscoelastic elements, suspended in plasma, a Newtonian fluid. The ESL is represented as a porous medium, and plasma flow in the layer is computed using the Brinkman approximation. It is shown that an initially circular cell positioned close to the ESL in a shear flow is deformed into an asymmetric shape. This breaking of symmetry leads to migration away from the wall. With increasing hydraulic resistivity of the layer, the rate of lateral migration increases. It is concluded that mechanical interactions of RBCs flowing in microvessels with a porous wall layer may reduce the rate of lateral migration and hence reduce the width of the cell-depleted zone external to the ESL, relative to the cell-depleted zone that would be formed if the interface between the ESL and free-flowing plasma were replaced by an impermeable boundary.

Key words: blood flow, capsule/cell dynamics, flow–vessel interactions

1. Introduction

Resistance to blood flow in microvessels has been studied since the time of Poiseuille in the nineteenth century (Poiseuille 1835, 1846). Flow resistance can be expressed in terms of the apparent viscosity, i.e. the viscosity of a Newtonian fluid that would result in the same flow rate for a given driving pressure. Observations in narrow glass tubes show a marked decrease in the apparent viscosity with decreasing diameter below 1000 μm, a phenomenon known as the Fåhraeus–Lindqvist effect (Fåhraeus & Lindqvist 1931; Pries, Neuhaus & Gaehtgens 1992). This reflects the non-continuum behaviour of blood near the tube wall, leading to the formation of a cell-free or cell-depleted layer. A simple two-layer model, in which the red blood cells (RBCs) are contained within a concentric cylindrical core region with relative diameter λ

† Email address for correspondence: secomb@u.arizona.edu

and with uniform viscosity μ_{core}, and the surrounding cell-free annular wall layer has viscosity μ_p, predicts apparent viscosity as $\mu_{app} = \mu_p/(1 - \lambda^4(1 - \mu_p/\mu_{core}))$ (Vand 1948; Secomb 1995). Because of the fourth-power dependence in this relationship, even a relatively narrow plasma layer (λ slightly less than unity) causes a substantial reduction in apparent viscosity. Physically, the presence of such a layer decreases the viscosity in the region near the wall where the shear rate is highest and where viscous energy dissipation would otherwise be concentrated.

Experimental studies of blood flow in microvascular networks reveal major differences from predictions based on *in vitro* observations of apparent viscosity (Pries *et al.* 1994). The main cause of these differences is the presence of a relatively thick layer, ~1 μm wide, of macromolecules bound to the endothelial cells lining microvessel walls (Pries, Secomb & Gaehtgens 2000). The volume fraction of macromolecules in this gel-like endothelial surface layer (ESL) is very low, probably much less than 1 % (Secomb, Hsu & Pries 1998). Even so, the ESL impedes the flow of plasma and substantially increases flow resistance in microvessels, relative to the values expected from data from glass tubes corresponding to the anatomical diameters of the vessels. The presence of the ESL also reduces the volume fraction of RBCs in microvessels (tube haematocrit), and affects interactions of blood cells with vessel walls. The layer may shield RBCs from large stresses when the cells traverse irregular capillary geometries during passage through the microcirculation (Secomb, Hsu & Pries 2002).

Blood is a concentrated suspension of cells, mainly red blood cells (RBCs), in plasma. The haematocrit (volume fraction of RBCs) is normally 40–45 %. The unstressed shape of a normal human RBC is a biconcave disc with a diameter of ~8 μm and a thickness of ~2 μm. The interior is a concentrated haemoglobin solution, which behaves as an incompressible viscous fluid. The cell membrane is viscoelastic, with low resistance to bending and in-plane shear deformations. As a consequence of these physical properties, RBCs are highly deformable, allowing blood to flow readily through microvessels despite being a concentrated suspension of particles with unstressed diameters comparable with microvessel diameters.

The physical mechanisms that determine the width of the cell-free or cell-depleted layer when blood flows in microvessels have been examined in several previous studies. In capillaries with diameters up to ~8 μm, RBCs frequently flow in single file. In such vessels, RBCs are compressed into narrow bullet-like shapes, and their mechanics can be analysed by assuming that the RBC has axisymmetric geometry. A further simplification is the use of lubrication theory to describe the motion of the suspending fluid in the layer between the cell and the vessel wall. Under these assumptions, the fluid–solid interaction problem can be expressed as a nonlinear system of ordinary differential equations, which can be solved numerically to predict cell shapes and apparent viscosity (Secomb *et al.* 1986). The width of the lubrication layer between the cell and the wall and the resulting apparent viscosity are predicted by this theory. Predictions agree well with experimental measurements in capillary-sized glass tubes. For tube diameters above ~8 μm, theoretical analyses must consider multiple interacting RBCs. This is a challenging computational problem, particularly if fully three-dimensional geometries are considered. The availability of increasing computing power in recent years has led to an upsurge of interest in this area (Dupin *et al.* 2007; Pivkin & Karniadakis 2008; McWhirter, Noguchi & Gompper 2009; Doddi & Bagchi 2009). For tube diameters above 30 μm, a good fit to experimental results is obtained from the two-layer model mentioned above, by assuming a cell-free layer width of 1.8 μm and $\mu_{core}/\mu_p = 3.3$ (Secomb 1995). This estimate for

the effective width of the cell-free layer is consistent with results of recent three-dimensional multi-cell simulations (Fedosov *et al.* 2010; Pan, Caswell & Karniadakis 2010).

Despite the inherent complexity of multi-RBC flows in microvessels, several physical phenomena can be identified that influence the lateral migration of cells (Goldsmith 1971; Secomb 2003). The formation of a cell-free or cell-depleted layer results from the tendency of flexible particles, including RBCs, to migrate away from the walls of a flowing channel. This migration is the focus of the present study. In the absence of inertial effects, the possible fluid mechanical causes for migration are interactions of the particle with the wall and with the non-uniform shear rate in channel flow (Coupier *et al.* 2008). The presence of a solid wall near the cell introduces an asymmetry in the forces on the cell, which can cause migration of deformable cells, for example as result of tank-treading motion for a spheroidal cell (Olla 1997) or the breaking of fore–aft symmetry in cell shape (Cantat & Misbah 1999; Sukumaran & Seifert 2001). Analyses of vesicles bound to a surface show the generation of lift forces due to asymmetry of vesicle shape or orientation (Cantat & Misbah 1999; Seifert 1999). In three-dimensional simulations, Pozrikidis (2005) showed the deformation and drift towards the centre-line of an initially spherical flexible particle placed in an eccentric position within a cylindrical tube. The dependence of migration rate of vesicles on lateral position has been studied experimentally and in simulations (Coupier *et al.* 2008). In each case, the migration is away from the wall. Even in the absence of wall effects, the nonlinear velocity profile resulting from flow driven by a pressure gradient can result in lateral migration towards the centre of the flow (Kaoui *et al.* 2008).

In a concentrated suspension such as blood, the formation of a region of low concentration near the wall as a result of lateral migration is counteracted by the phenomenon of 'shear-induced diffusion'. The quasi-random effects of hydrodynamic interactions of each cell with many other cells result in a tendency for net migration down the concentration gradient, towards the wall (Goldsmith 1971; Leighton *et al.* 1987). The width of the cell-depleted layer that evolves as the flow travels along the channel is dictated by the balance between the tendency to migrate away from the wall and the effect of shear-induced dispersion. With increasing haematocrit, the latter effect becomes stronger, leading to reduction in the width of the cell-depleted layer, as observed experimentally (Maeda *et al.* 1996).

In a study motivated by the goal of understanding the effects of the ESL on cell trajectories, Beaucourt, Biben & Misbah (2004) analysed the interactions of rigid and deformable vesicles with a compressible but impermeable wall substrate, subject to a linear shear flow. Depending on the substrate stiffness, a lateral lift force is generated for rigid circular particles, whereas the reversibility of Stokes flow implies that no such force would be generated if the layer were incompressible.

The effects of a porous wall layer on lateral migration of deformable particles do not appear to have been examined in any previous study. The goal of the present study is to examine the transverse migration of RBCs lying near the wall, and how this is affected by the presence of the ESL, considered as a porous medium. We consider the motion and deformation of a single cell with an initial position close to the layer in a parallel-sided channel. The plasma flow within the layer is analysed using the Brinkman approximation. The RBC is represented using a simplified two-dimensional model that has previously been shown to yield behaviour in good agreement with

in vitro and *in vivo* experimental results. The results are discussed in terms of their significance for the development of the cell-depleted layer in microvessels.

2. Methods

2.1. *Modelling approach*

In the present study, a simplified two-dimensional model is used to represent the motion and deformation of the RBC (Secomb, Styp-Rekowska & Pries 2007; Barber *et al.* 2008). Two-dimensional models have been used in a number of previous theoretical studies of deformation and lateral migration of vesicles and RBCs in channel flow (Secomb & Skalak 1982; Cantat & Misbah 1999; Beaucourt *et al.* 2004; Freund 2007; Kaoui *et al.* 2008; Kaoui, Biros & Misbah 2009). Such models allow representation of the main fluid mechanical phenomena involved, including the effects of shear flow, proximity to boundaries, cell deformation, cell tumbling and cyclic 'tank-treading' motion of the membrane around the cell interior. The latter behaviour is observed when an RBC is placed in simple shear flow of a high-viscosity fluid. In this context, a potential limitation of two-dimensional models for RBCs is that tank-treading motion then requires only bending deformation of the membrane. A three-dimensional RBC necessarily experiences in-plane shear deformation during tank-treading, as bands of membrane around the cell are alternately lengthened and shortened. This continuous deformation results in viscous energy dissipation in the membrane (Fischer 1980). Neglect of the effect of membrane viscosity leads to overestimation of tank-treading rates (Hsu & Secomb 1989; Fedosov *et al.* 2010).

The model used here is designed to overcome this limitation. The cross-sectional shape of the RBC is represented by a set of viscoelastic elements on the perimeter of the cell, together with a set of viscous elements in the interior (Secomb *et al.* 2007) as shown in figure 1(*a*). The external elements represent the viscoelastic response of the RBC membrane to elongation and shortening: the viscous component represents the viscosity of the lipid bilayer and the elastic component represents the elasticity of the cytoskeletal protein network. The internal elements represent both the viscosity of the cell's interior and the cell membrane's viscous resistance to three-dimensional out-of-plane deformations, as occur during tank-treading. Membrane bending elasticity is represented by an elastic resistance at the nodes. The incompressibility of the RBC interior is represented approximately in the model by assigning an internal pressure that depends on the area of the model cell. The suspending medium is a viscous incompressible fluid. In the approach used here, the equations of mechanical equilibrium are imposed exactly at each node. This approach was taken to minimize numerical errors that could affect the predicted lateral migration of cells, as could arise if the continuum equations of the membrane were represented in discrete form. A finite-element method is used to compute the flow external to the cell, simultaneously with the equations of equilibrium at the nodes of the model cell.

This method was used to simulate the tank-treading of RBCs in simple shear flow of a high-viscosity (13 cP) medium (Secomb *et al.* 2007). The predicted variations of cell elongation and tank-treading frequency with shear rate were compared with experimental data (Fischer, Stohr & Schmid-Schönbein 1978; Secomb 2003). With suitably chosen values of the viscous and elastic parameters, this model closely approximated the corresponding experimental data. If the internal viscous elements were not included in the model, no such agreement could be obtained for any choice of the parameter values. The model was then used to simulate the motion of RBCs in microvessels (Secomb *et al.* 2007). When placed in off-axis positions, the cells

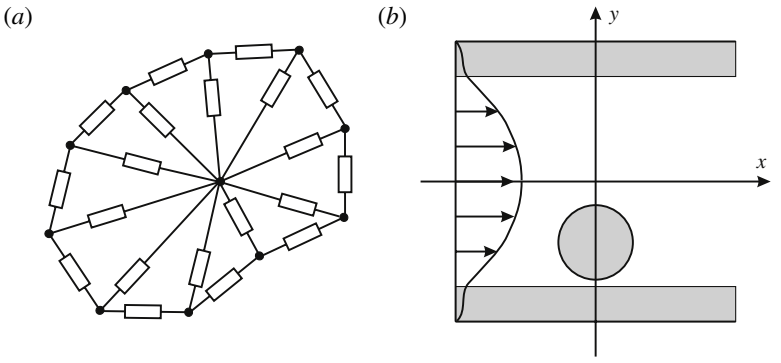

FIGURE 1. (*a*) Two-dimensional model for the RBC. Rectangles represent viscoelastic elements. (*b*) Geometry of the system to be analysed. Shaded areas adjacent to channel boundaries represent the ESL. The shaded circle represents the RBC. A typical velocity profile in the channel is indicated.

assume asymmetric shapes and migrate towards the centre-line. Computed cell shapes and centre-of-mass trajectories showed good quantitative agreement with experimental observations obtained by intravital microscopy of the rat mesentery. Applications of this model to study the motion of RBCs in diverging bifurcations and the migration of RBCs initially positioned near the wall of a flowing parallel-sided channel have been reported previously (Barber *et al.* 2008; Secomb 2010).

2.2. *Equations of fluid flow*

Blood vessels are represented in two dimensions as uniform channels of width 10 or 20 μm. The ESL region is assumed to be a layer of uniform width lining each boundary, as shown in figure 1(*b*). Additional simulations are performed to show the effect of a linear shear flow. In this case, parallel boundaries 20 μm apart are used. The suspending medium is assumed to be an incompressible fluid with zero Reynolds number, so that the inertial effects of flow can be neglected and the governing equations are those of Stokes flow. The pressure and velocity components fields are expressed in two-dimensional coordinates (x, y) as $p(x, y)$ and $\boldsymbol{u}(x, y)$ where $\boldsymbol{u} = (u, v)$. The components of stress are

$$\sigma_{xx} = 2\mu\frac{\partial u}{\partial x} - p, \quad \sigma_{xy} = \mu\left(\frac{\partial u}{\partial y} + \frac{\partial v}{\partial x}\right), \quad \sigma_{yy} = 2\mu\frac{\partial v}{\partial y} - p, \tag{2.1}$$

where μ is the fluid viscosity.

The ESL consists of a gel-like assembly of macromolecules with a low solid volume fraction, anchored to the vessel wall. According to existing concepts (Pries *et al.* 2000), the resistance of the ESL to compression results from osmotic swelling, which generates tension in the molecular chains that extend from the wall. When exposed to shear stress, the strands in the layer are displaced from a perpendicular direction (on average) from the wall, allowing transmission of the shear stress to the wall by the strands. The majority of the fluid shear stress acting on endothelial cells is thus transmitted by the ESL (Secomb, Hsu & Pries 2001). In the present model, the ESL is therefore represented as a porous medium. The fluid flow in the layer is computed using the Brinkman approximation (Brinkman 1947), such that the ESL imposes a drag term on the fluid proportional to the local fluid velocity. Hydrostatic pressure is

continuous across the edge of the layer, and variations in pressure do not result in compression or expansion of the layer. Cases in which the RBC enters the layer are not considered here. The effects of transient deformation of the ESL, here neglected, have been analysed previously (Secomb *et al.* 2001). The equations for equilibrium of stresses then yield

$$\frac{\partial \sigma_{xx}}{\partial x} + \frac{\partial \sigma_{xy}}{\partial y} = \kappa u, \quad \frac{\partial \sigma_{xy}}{\partial x} + \frac{\partial \sigma_{yy}}{\partial y} = \kappa v, \tag{2.2}$$

where κ is the hydraulic resistivity, which is taken to be zero outside the ESL and a uniform positive value inside the ESL. The divergence of the velocity field is given by

$$e = \frac{\partial u}{\partial x} + \frac{\partial v}{\partial y}, \tag{2.3}$$

with $e = 0$ since the fluid is incompressible. The boundary conditions are no-slip conditions on solid boundaries, and continuity of fluid velocity and stress across the boundary between the ESL and free plasma.

2.3. *Simulation of red blood cells*

RBCs are represented in two dimensions in terms of their cross-sections in a plane through the centre of the cell. The cell membrane is modelled as a chain of straight elements connected at nodes. Each element consists of viscous and elastic components connected in parallel, to represent the viscoelastic response of the cell membrane. The nodes at which the elements are connected are taken to be elastic, and thus represent the cell membrane's resistance to bending. This model also includes a central node that is connected to all external nodes by viscous elements, representing the effects both of the internal viscosity of the cell and also of the viscous resistance of the cell membrane to the out-of-plane components of the deformation, as already discussed (Secomb *et al.* 2007).

The nodes and elements are numbered successively, $i = 1, \ldots, n$, where n is the total number of external nodes. The external elements and nodes of the model cell have forces acting on them as a result of the fluid flow. Consequently, the longitudinal (tension) force $t_i(s)$, transverse (shear) force $q_i(s)$, and bending moment $m_i(s)$ acting in the external element i are functions of distance s along the element from the node i to node $i + 1$, where $0 \leqslant s \leqslant l_i$ and l_i is the length of the external element i. The equations of mechanical equilibrium are

$$\frac{\mathrm{d}t_i}{\mathrm{d}s} = -g_i, \quad \frac{\mathrm{d}q_i}{\mathrm{d}s} = -f_i, \quad \frac{\mathrm{d}m_i}{\mathrm{d}s} = q_i, \tag{2.4}$$

where $f_i(s)$ and $g_i(s)$ are the normal and tangential components of the fluid loading.

The interior of a three-dimensional RBC is effectively incompressible, so that it deforms at constant volume, and the membrane deforms at nearly constant surface area. In two dimensions, the analogous properties are the perimeter and area in the model-cell plane. These properties are not kept constant, but are constrained such that they lie within a narrow range that would represent the possible shapes of a three-dimensional cell with fixed surface area and volume. In the model, variations of perimeter are resisted by the elasticity of the external elements (see below), and variations of cell area A are resisted by assigning an interior pressure to the cell:

$$p_{int} = k_p(1 - A/A_{ref}), \tag{2.5}$$

where A_{ref} and k_p are constants.

The normal and shear components of the stresses acting on external segment i are then given by

$$f_i = -p_{int} - \sigma_{xx}\sin^2\theta_i + 2\sigma_{xy}\sin\theta_i\cos\theta_i - \sigma_{yy}\cos^2\theta_i, \tag{2.6}$$

$$g_i = (\sigma_{xx} - \sigma_{yy})\sin\theta_i\cos\theta_i - \sigma_{xy}(\cos^2\theta_i - \sin^2\theta_i), \tag{2.7}$$

where θ_i is the angle of the element i relative to the x-axis.

In developing the equations for equilibrium at each node, it is useful to define the mean longitudinal and transverse force in segment i as

$$\bar{t}_i = \frac{1}{l_i}\int_0^{l_i} t_i(s)\,\mathrm{d}s, \quad \bar{q}_i = \frac{1}{l_i}\int_0^{l_i} q_i(s)\,\mathrm{d}s. \tag{2.8}$$

The external elements forming the cell are viscoelastic with constitutive properties defined by

$$\bar{t}_i = k_t\left(\frac{l_i}{l_0} - 1\right) + \mu_m\frac{1}{l_i}\frac{\mathrm{d}l_i}{\mathrm{d}t} \tag{2.9}$$

for the external elements, where l_0 is the reference length of the element, k_t is the elastic modulus and μ_m is the viscosity. The length changes occurring in the cases considered here are not large, and a linear elastic model is used for simplicity. The internal elements are assumed to have viscous resistance to changes in length, giving a tension

$$T_i = \mu'_m\frac{1}{L_i}\frac{\mathrm{d}L_i}{\mathrm{d}t}, \tag{2.10}$$

where L_i is the length of the internal element i and μ'_m is its viscosity.

The bending resistance of the membrane is represented by introducing bending moments at each node:

$$m_i(0) = -\frac{k_b\alpha_i}{l_0}, \quad m_i(l_i) = -\frac{k_b\alpha_{i+1}}{l_0}, \tag{2.11}$$

where k_b is the bending modulus and $\alpha_i = \theta_i - \theta_{i-1}$ is the angle between elements $i-1$ and i. Integrating the above equation for $\mathrm{d}m_i/\mathrm{d}s$ gives

$$\bar{q}_i = \frac{k_b(\alpha_i - \alpha_{i+1})}{l_i l_0}. \tag{2.12}$$

By integration by parts, the loads acting on the endpoints of the elements, $q_i(0)$, $q_i(l_i)$, $t_i(0)$ and $t_i(l_i)$, can each be expressed as a sum of the mean longitudinal or transverse force, $\bar{t}_i$ or $\bar{q}_i$, and an integral of the fluid stress $f_i(s)$ or $g_i(s)$. For example,

$$q_i(0) = \bar{q}_i + \frac{1}{l_i}\int_0^{l_i} f_i(s)(l_i - s)\,\mathrm{d}s. \tag{2.13}$$

The equations for equilibrium of forces at node i are

$$t_i(0)\cos\theta_i - t_{i-1}(l_{i-1})\cos\theta_{i-1} - q_i(0)\sin\theta_i + q_{i-1}(l_{i-1})\sin\theta_{i-1} + T_i\cos\phi_i = 0, \tag{2.14}$$

$$t_i(0)\sin\theta_i - t_{i-1}(l_{i-1})\sin\theta_{i-1} + q_i(0)\cos\theta_i - q_{i-1}(l_{i-1})\cos\theta_{i-1} + T_i\sin\phi_i = 0, \tag{2.15}$$

where ϕ_i is the angle of the internal element i from the x-axis. Equilibrium of forces at the central node results in

$$\sum_{i=1}^{n} T_i \cos\phi_i = \sum_{i=1}^{n} T_i \sin\phi_i = 0. \tag{2.16}$$

The equilibrium equations for a given configuration of the cell can thus be expressed as a linear system involving the fluid loadings f_i and g_i on each external element and the velocities of the nodes. The resulting coupled system of equations is used to compute the cell's motion.

2.4. *Computational method*

The system of coupled equations for the motion of the cell and the surrounding fluid is solved using a finite-element package (FlexPDE, version 5.1.4, PDE Solutions Inc., Antioch, CA). Quadratic elements are used. Because of the structure of FlexPDE, the incompressibility condition $e = 0$ cannot be specified, but instead the condition

$$\nabla^2 p = Ke, \tag{2.17}$$

where K is a large value, approximately satisfies the condition. Generally, $n = 20$ nodes are used to represent the RBC. At each time step, the nodal velocities are computed using the FlexPDE package. The cell shapes are then updated using the computed nodal velocities and specified time step, using an explicit Euler scheme. Numerical error in the calculation of the velocity field is controlled by the FlexPDE package, which automatically refines the domain's mesh until the solution errors are within a specified tolerance. The integration with respect to time is performed using an explicit Euler scheme. The time step must be set very small to avoid numerical instability, which results primarily from the stiff constraint on cell area. The time steps used, 0.5 ms for channel flow and 0.25 ms in the case of shear flow, are also sufficiently small that the errors resulting from the use of an explicit scheme for time integration are negligible.

2.5. *Parameter values and initial conditions*

The procedures for setting the dimensions and material parameters of the cell were described previously (Secomb *et al.* 2007; Barber *et al.* 2008). The experimentally determined shear elastic modulus, shear viscosity and bending resistance of the membrane are 6×10^{-6} N m^{-1}, 10^{-6} N s m^{-1} and 1.8×10^{-19} N m, respectively (Evans 1983; Hochmuth & Waugh 1987). However, these values are not directly applicable to the discrete two-dimensional representation of the cell. Therefore, the parameters were chosen so that predictions closely matched experimental results for RBCs tank-treading in a high-viscosity medium (Fischer *et al.* 1978; Secomb 2003). The resulting values were $k_t = 1.2 \times 10^{-5}$ N m^{-1} representing membrane shear elasticity, $\mu_m = 2 \times 10^{-7}$ N s m^{-1} representing membrane viscous resistance to in-plane deformation, $\mu'_m = 10^{-7}$ N s m^{-1} representing effects of internal viscosity and of membrane viscous resistance to out-of plane deformation, reference segment length $l_0 = 0.97$ μm with 20 nodes, and reference cell area $A_{ref} = 22.2$ μm^2. The fluid viscosity is assumed to be $\mu = 10^{-3}$ Pa s. An ESL width of $w = 1$ μm is assumed (Secomb *et al.* 1998). A dimensionless measure of hydraulic resistivity can be defined as $\bar{\kappa} = \kappa w^2/\mu$. Four different cases are considered with respect to the properties of the ESL: no layer; layer with low hydraulic resistivity $\kappa = 10^{10}$ N s m^{-4} ($\bar{\kappa} = 10$); layer with high hydraulic resistivity $\kappa = 10^{11}$ N s m^{-4} ($\bar{\kappa} = 100$); and impermeable

layer, equivalent to a channel of width 8 μm with no layer. Secomb *et al.* (1998) estimated that the actual hydraulic resistivity in normal capillaries is 10^{11} N s m^{-4} or more. In abnormal situations such as haemodilution, the ESL hydraulic resistivity may be attenuated (Pries *et al.* 1998).

In the simulations presented here, the initial condition for the cell shape is chosen to be a circle with radius 2.66 μm, giving an area equal to A_{ref}. Although the static equilibrium shape of a human RBC is a biconcave disc, the position of the dimple relative to the cell membrane changes readily during tank-treading motions with a relatively small change in stored elastic energy (Fischer 2004). The use of a circular reference shape is therefore more appropriate than choosing a biconcave reference shape. The initial perimeter of the cell is 16.7 μm, or 86 % of the perimeter if all 20 exterior segments were at their reference lengths. During the initial phase of the motion, the perimeter increases, allowing the cell to achieve non-circular shapes at constant area.

3. Results

Sequences of computed cell shapes are shown in figure 2, for a cell initially placed with its centre 0.9 μm from the centre-line in a channel of width 10 μm. The computational domain is 20 μm in length, centred on the particle. A pressure gradient of 10^5 Pa m^{-1} is imposed in each case. In the absence of a particle, this would generate centre-line velocities in the range 0.8 mm s^{-1} (impermeable layer) to 1.25 mm s^{-1} (no layer) for the four cases considered. Predicted particle velocities are generally in the range 0.5–1 mm s^{-1}. Supplementary movies showing the motion and deformation of the cell for each case, for a simulated period of 500 ms, are available at journals.cambridge.org/flm.

The primary finding is that the cell in all cases drifts towards the centre-line of the channel. Well-known symmetry arguments, based on the time reversibility of Stokes flow, show that a rigid circular particle would not exhibit any transverse motion within a parallel-sided channel. Any transverse migration is therefore a consequence of the shape change of the flexible particle. The direction and rate of migration depend on the deformed shape and orientation of the particle. When the four cases illustrated in figure 2 are compared, it is evident that the shape change of the particle during the initial phase of the motion (the first 20 ms) becomes more pronounced with increasing resistivity of the ESL. These small differences in shape are most noticeable at the trailing edge of the cell close to the wall. Of particular note is the generation of an S-shaped profile, a lift-generating configuration, in the portion of the cell adjacent to the vessel wall (Skotheim & Mahadevan 2005). At later times, the cells tend towards similar shapes in all four cases.

To assess the deformation and orientation of the cell shape in more detail, the two-dimensional moment-of-inertia tensor is used:

$$\boldsymbol{I} = \begin{pmatrix} I_{xx} & I_{xy} \\ I_{yx} & I_{yy} \end{pmatrix}, \tag{3.1}$$

where

$$I_{xx} = \sum_{i=1}^{n} y_i^2, \quad I_{yy} = \sum_{i=1}^{n} x_i^2, \quad I_{xy} = -\sum_{i=1}^{n} x_i y_i. \tag{3.2}$$

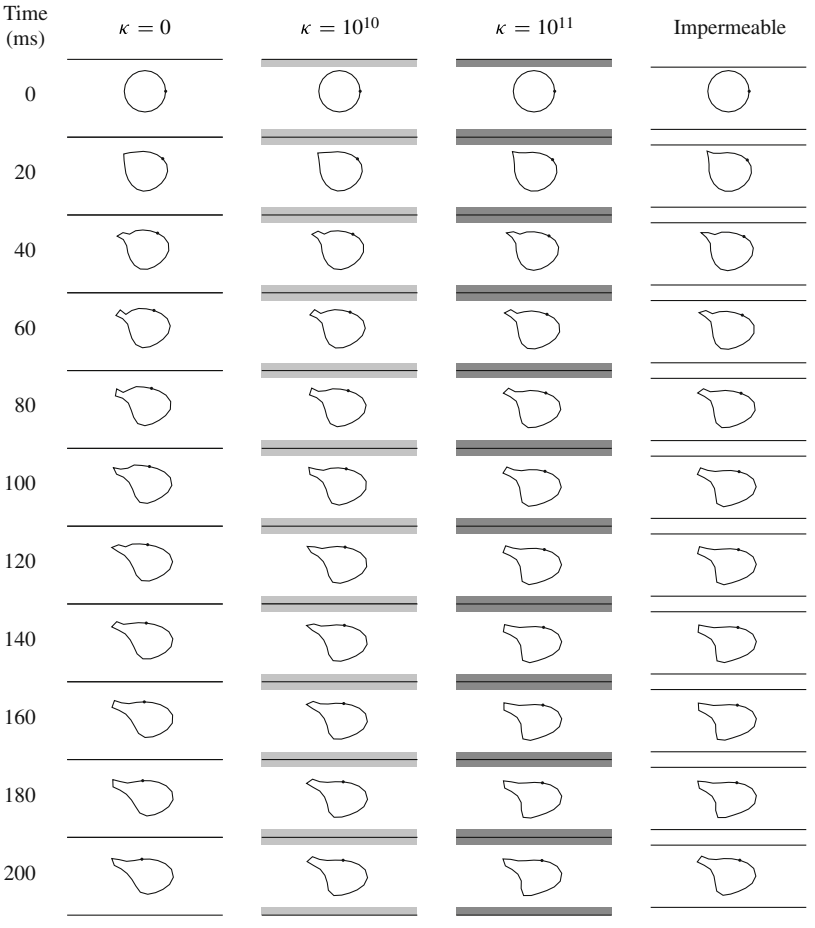

FIGURE 2. Motion and deformation of a cell initially placed at 0.9 μm from the centre-line, shown at 20 ms intervals for four different cases, as indicated. Total channel width is 10 μm (8 μm in the impermeable case). Lines show channel boundaries. Shading shows location of permeable ESL. The hydraulic resistivity κ of the ESL is in N s m^{-4}.

Here (x_i, y_i) are the coordinates of external node i. The eigenvalues and eigenvectors of $\boldsymbol{I}$ are computed. The inclination is defined as the angle between the channel axis and eigenvector corresponding to the major axis of the shape. The eigenvalues are normalized with respect to the (equal) eigenvalues of the undeformed shape, giving indices of deformation in the directions of the major and minor axes.

The variations with time of these parameters are shown in figure 3(*a*,*b*). The eigenvalues of $\boldsymbol{I}$ and the inclination of the major axis show similar behaviour in all four cases. During the initial phase of the motion, the larger eigenvalue of $\boldsymbol{I}$ increases. This increase is most rapid in the case of an impermeable boundary. At the outset, the major principal axis of the cell shape is inclined at almost 45° to the channel axis. This reflects the fact that the principal axis of the straining component of a simple shear flow is at 45° to the flow direction. The inclination decreases with time, as a consequence of the rotational component of the shear flow. In all cases, the centre of mass moves towards, but does not reach, the channel centre-line (figure 3*c*).

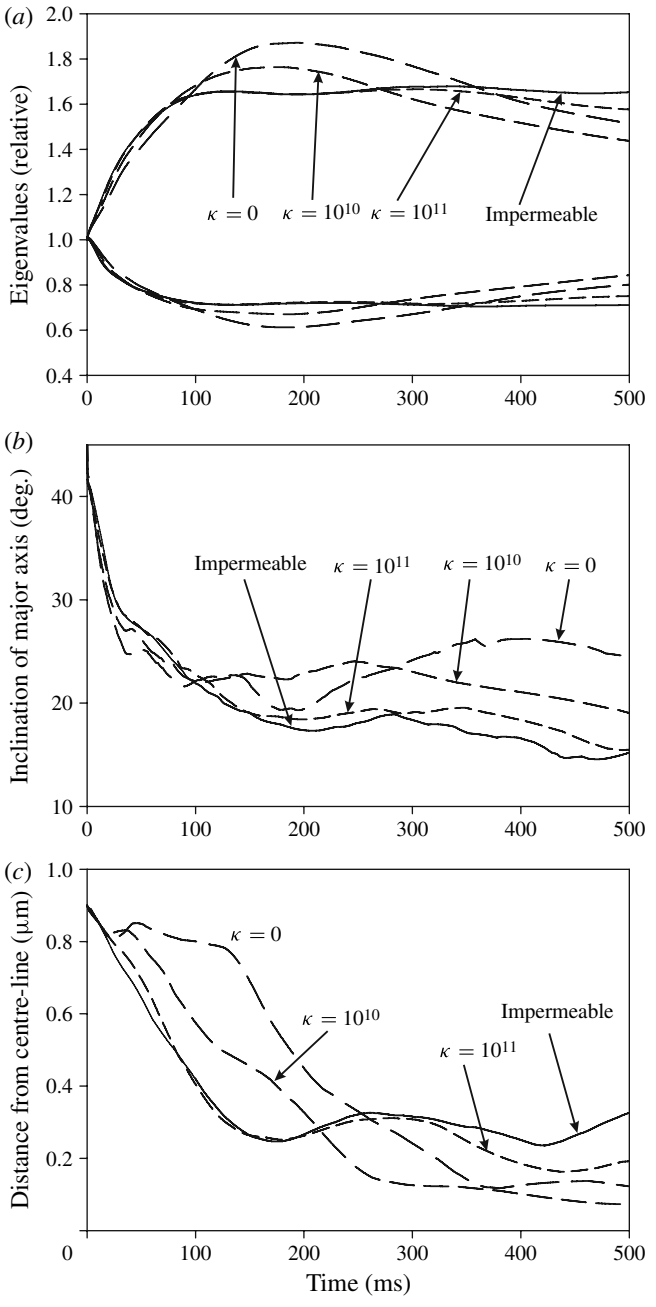

FIGURE 3. Motion and deformation of a flexible cell initially placed at 0.9 μm from the centre-line. (*a*) Eigenvalues of shape (see text). (*b*) Inclination of major principal axis. (*c*) Distance of centre of mass from centre-line. The hydraulic resistivity κ of the ESL is in N s m^{-4}.

The remaining offset from the centre-line reflects the asymmetry in the eventual cell shape. During a short initial phase of the motion (∼20 ms), the lateral migration is approximately independent of the layer permeability. However, the motion during

the subsequent 200 ms is strongly influenced by the layer properties, with slower migration in the absence of a layer and more rapid migration for an impermeable layer and for a layer permeability of 10^{11} N s m^{-4}.

The effect of channel width on particle migration from the wall is explored in figure 4, for channel widths of 10 and 20 μm, and for a linear shear flow, corresponding to the limit of infinite width. In each case, the particle centre is initially 4.1 μm from the wall. The migration is again almost independent of layer permeability during the initial 20 ms, but generally decreases with increasing permeability at later times. The behaviour shows a number of changes with increasing channel width. In a wider channel, the particle centre of mass moves towards the wall in the initial phase of the motion. This difference reflects the fact that the entire particle is subjected to the shear flow in the case of a 20 μm channel and a shear flow, whereas the particle lies across the centre-line of the 10 μm channel. As shown by the insets, the cell therefore tends to be flattened close to the wall in the initial phase. In the subsequent motion, the migration away from the wall is much more pronounced in the 20 μm channel and in the shear flow than in the 10 μm channel. This suggests that the curvature of the velocity profile is not one of the main factors responsible for transverse migration in the cases considered here. Tumbling of the RBC is predicted in the 20 μm channel and in the shear flow but not in the 10 μm channel. As would be expected, tumbling tends to occur when the cell is immersed in a velocity gradient that does not change sign, but is inhibited by proximity to an impermeable or nearly impermeable boundary. In the tumbling regime, continuous changes in cell shape result in apparently non-periodic motion and no steady regime is reached. In some cases, simulations were terminated when a node angle α_i approached $\pm\pi$.

Further insight into the effect of the wall layer and its properties on the deformation of the particle can be obtained by considering the distribution of stresses acting on the particle at the initial instant of the flow. For clarity, we restrict attention to a rigid circular particle. Figure 5 shows the distributions of normal and shear stress acting on the circumference of the particle, obtained using FlexPDE as already described. As before, four cases are considered with respect to the properties of the ESL. As would be expected, the stresses on the particle are largest in the region near the point of narrowest gap, and the magnitude of the stresses increases with increasing hydraulic resistivity of the layer. The consequences of these force distributions for particle deformation are discussed below.

4. Discussion

The transverse migration of RBCs, leading to the formation of a cell-depleted layer, has important implications for the resistance to blood flow in the microcirculation, yet the mechanisms responsible for this migration remain incompletely understood. The walls of microvessels *in vivo* are lined with a relatively thick (∼1 μm) gel-like layer of macromolecules (ESL) that has a major impact on flow resistance. The effect of the ESL on the transverse migration of RBCs flowing in microvessels does not appear to have been addressed previously.

The width of the cell-depleted layer in a microvessel depends on the balance between two effects: the tendency of individual RBCs to move away from the wall; and the tendency of RBCs to be driven out of the concentrated central region towards the more dilute region at the wall. This latter effect probably occurs as a result of shear-induced diffusion (Leighton *et al.* 1987). Frequent hydrodynamic interactions occur between cells that are travelling with different speeds in a shear flow and

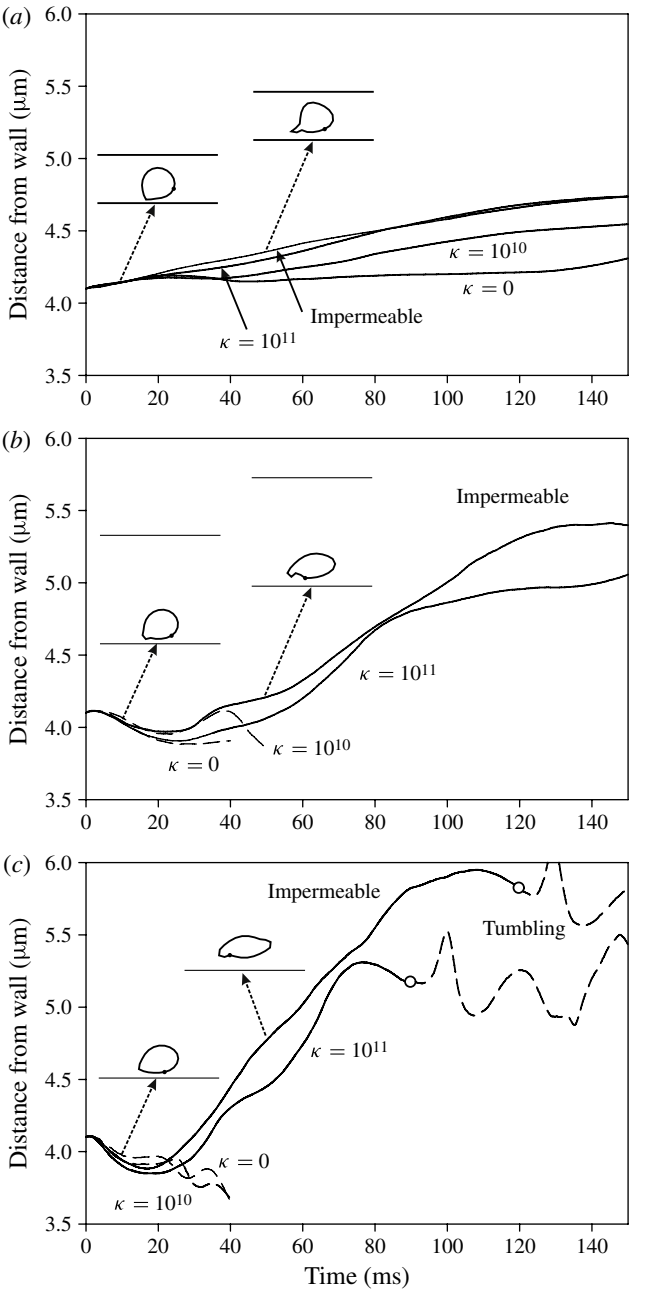

FIGURE 4. Distance of particle centre of mass from wall: comparison of channel flow and shear flow. (*a*) Flow in a 10 μm channel lined by a 1 μm permeable layer, with pressure gradient 10^5 Pa m^{-1} as in figures 2 and 3. (*b*) Flow in a 20 μm channel lined by a 1 μm permeable layer, with pressure gradient 5×10^4 Pa m^{-1}. (*c*) Linear shear flow (500 s^{-1}) over a wall lined by a 1 μm permeable layer. Solid curves denote motion with stable particle orientation, and dashed curves indicate tumbling motion. Open circles show approximate time of transition to tumbling. Insets show predicted particle shapes 10 ms and 50 ms after initiation of the motion, for the case of an impermeable layer. The hydraulic resistivity κ of the ESL is in N s m^{-4}.

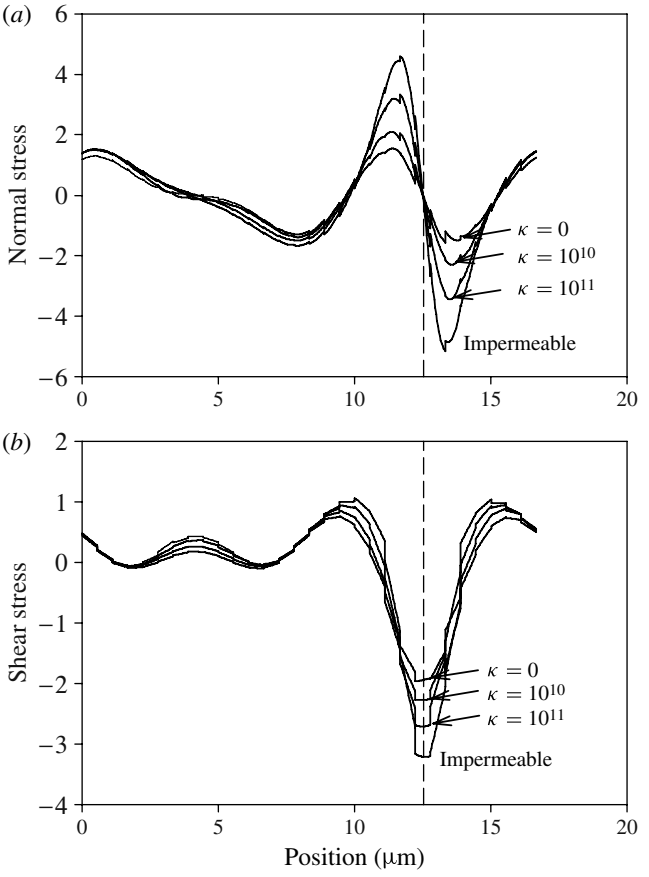

FIGURE 5. Distribution of dimensionless fluid stresses acting on the boundary of a rigid circular particle of radius 2.66 μm placed at 0.9 μm from the centre-line of a 10 μm channel lined by a 1 μm permeable layer: (*a*) normal stress; and (*b*) shear stress. Layer properties for each case are as in figures 2 and 3. The horizontal axis shows distance around the particle, starting from the point at the extreme right side of the particle. The vertical line shows location of point of minimum gap width. Irregularity in curves results from the calculation of stress by differentiation of velocity in the finite-element scheme. The hydraulic resistivity κ of the ESL is in N s m^{-4}.

'collide' with each other. During such interactions, cells are displaced laterally, and occasionally cells are thereby driven close to the vessel wall. The initial condition assumed here can be considered to represent such a case, as discussed further below. The analysis of shear-induced diffusion in RBC suspensions presents a significant challenge in understanding microvascular blood rheology, but this topic is not pursued further here.

In this study, we consider the migration of an individual RBC away from a wall in channel flow. In such a flow, RBCs undergo large deformations while simultaneously tumbling and/or tank-treading (Secomb 2010). Here, we have focused on the initial stage of this motion, about which some general conclusions can be drawn. When an initially circular particle closely approaches the vessel wall, relatively large stresses are generated on the part of the particle boundary closest to the wall. The distribution

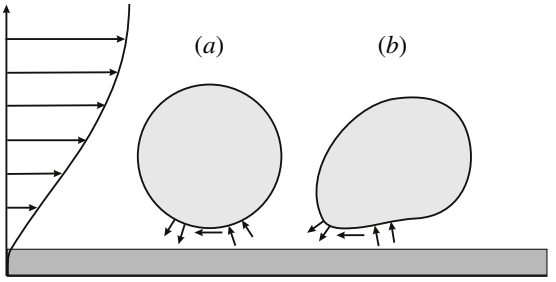

FIGURE 6. Diagram showing forces acting on freely suspended particles in a channel flow near a boundary. Arrows near particle indicate regions of high normal and shear stresses acting on the particle. (*a*) Initial circular particle. Regions of high stress correspond to those shown in figure 4. (*b*) Expected deformation of a flexible particle resulting from force distribution shown in panel (*a*). Regions of positive and negative normal stress and high shear stress result in deformation into a teardrop-like shape.

of forces on that point tends to deform the particle into a teardrop-like shape with an S-shaped profile adjacent to the wall, as illustrated in figure 6. This shape is aligned at a positive angle to the flow direction, considering both the overall shape (principal axis) and the boundary close to the wall. From well-known arguments of lubrication theory, such an inclination induces a lift that tends to drive the particle away from the wall (Cameron 1966; Secomb & Hsu 1993). The generation of lift by such a 'soft slider' has been analysed previously using lubrication theory (Skotheim & Mahadevan 2005). If a permeable wall layer is present, the migration increases with increasing hydraulic resistivity of the layer. Two causes for this effect are evident. Firstly, the initial deformation of the particle, leading to the characteristic S-shaped profile adjacent to the wall, is more pronounced if the layer is impermeable or nearly impermeable. Secondly, the lubrication forces that are generated within the lubrication layer are attenuated if the boundary is permeable.

In the analyses presented here, the initial shape was assumed to be circular. It could be argued that such a shape is not representative of the observed shapes of RBCs in flow. Regardless of the deformation of the cell, however, it maintains a curved profile as a result of the bending resistance of the cell membrane. The shape of the part of the RBC closest to the wall can be approximated as an arc of a circle, for which the arguments presented above would still apply. If a non-circular shape (such as an ellipse or a biconcave shape) were chosen for the initial shape, the particle migration would be strongly biased by the orientation of the principal axes of this shape, making the effects of flow-induced shape change more difficult to detect. An alternative, more computationally expensive, approach would be to perform simulations assuming such shapes and average the results over an ensemble of orientations.

Discussion of the effects of the ESL on particle migration requires definition of a reference configuration with no ESL, but the choice of this configuration is not unique. If a vessel of a given diameter were to shed its ESL, resulting in a vessel with larger effective diameter, the rate of migration of a cell at a given initial position would decrease, as indicated by the curves labelled '$\kappa = 0$' in figures 3 and 4. The loss of the ESL would result in a decreased vascular resistance and increased blood flow. All microvessels are subject to long-term structural adaptation of diameters such that blood flow is adjusted to meet tissue needs (Pries & Secomb 2008). In the long term, therefore, a biologically relevant reference configuration is one with approximately the

same flow resistance, i.e. with an internal diameter matching the diameter internal to the ESL of a normal vessel. This case is represented by the curves labelled 'impermeable' in figures 3 and 4.

In conclusion, we have examined the mechanics of RBC migration away from microvessel walls using a two-dimensional model, and considering the effects of an ESL, represented as a porous medium using the Brinkman approximation. The model predicts that RBCs that come close to the edge of the ESL have a tendency to migrate away from it, and that this tendency decreases as the ESL becomes more permeable. A reduction in transverse migration would be expected to result in decreased width of the cell-depleted layer external to the ESL in microvessels *in vivo*, relative to the cell-depleted layer that would form if the interface between the ESL and free-flowing plasma were replaced by an impermeable boundary.

Acknowledgement

This work was supported by NIH grant HL034555.

Supplementary movies are available at journals.cambridge.org/flm.

REFERENCES

BARBER, J. O., ALBERDING, J. P., RESTREPO, J. M. & SECOMB, T. W. 2008 Simulated two-dimensional red blood cell motion, deformation, and partitioning in microvessel bifurcations. *Ann. Biomed. Engng* **36**, 1690–1698.

BEAUCOURT, J., BIBEN, T. & MISBAH, C. 2004 Optimal lift force on vesicles near a compressible substrate. *Europhys. Lett.* **67**, 676–682.

BRINKMAN, H. C. 1947 A Calculation of the viscous force exerted by a flowing fluid on a dense swarm of particles. *Appl. Sci. Res.* A **1**, 27–34.

CAMERON, A. 1966 *The Principles of Lubrication*. Wiley.

CANTAT, I. & MISBAH, C. 1999 Lift force and dynamical unbinding of adhering vesicles under shear flow. *Phys. Rev. Lett.* **83**, 880–883.

COUPIER, G., KAOUI, B., PODGORSKI, T. & MISBAH, C. 2008 Noninertial lateral migration of vesicles in bounded Poiseuille flow. *Phys. Fluids* **20**.

DODDI, S. K. & BAGCHI, P. 2009 Three-dimensional computational modeling of multiple deformable cells flowing in microvessels. *Phys. Rev.* E **79**, 046318.

DUPIN, M. M., HALLIDAY, I., CARE, C. M., ALBOUL, L. & MUNN, L. L. 2007 Modeling the flow of dense suspensions of deformable particles in three dimensions. *Phys. Rev.* E **75**, 066707.

EVANS, E. A. 1983 Bending elastic modulus of red blood cell membrane derived from buckling instability in micropipet aspiration tests. *Biophys. J.* **43**, 27–30.

FÅHRAEUS, R. & LINDQVIST, T. 1931 The viscosity of the blood in narrow capillary tubes. *Am. J. Physiol.* **96**, 562–568.

FEDOSOV, D. A., CASWELL, B., POPEL, A. S. & KARNIADAKIS, G. E. 2010 Blood flow and cell-free layer in microvessels. *Microcirculation* **17**, 615–628.

FISCHER, T. M. 1980 On the energy dissipation in a tank-treading human red blood cell. *Biophys. J.* **32**, 863–868.

FISCHER, T. M. 2004 Shape memory of human red blood cells. *Biophys. J.* **86**, 3304–3313.

FISCHER, T. M., STOHR, M. & SCHMID-SCHÖNBEIN, H. 1978 Red blood cell (rbc) microrheology: Comparison of the behaviour of single rbc and liquid droplets in shear flow. In *Biorheology* (ed. C.-R. Huang & A. L. Copley). *AIChE Symposium Series No. 182,* vol. 74, pp. 38–45. American Institute of Chemical Engineers.

FREUND, J. B. 2007 Leukocyte margination in a model microvessel. *Phys. Fluids* **19**, 023301.

GOLDSMITH, H. L. 1971 Red cell motions and wall interactions in tube flow. *Fed. Proc.* **30**, 1578–1590.

HOCHMUTH, R. M. & WAUGH, R. E. 1987 Erythrocyte membrane elasticity and viscosity. *Annu. Rev. Physiol* **49**, 209–219.

HSU, R. & SECOMB, T. W. 1989 Motion of nonaxisymmetric red blood cells in cylindrical capillaries. *Trans. ASME: J. Biomech. Engng* **111**, 147–151.

KAOUI, B., BIROS, G. & MISBAH, C. 2009 Why do red blood cells have asymmetric shapes even in a symmetric flow? *Phys. Rev. Lett.* **103**, 188101.

KAOUI, B., RISTOW, G. H., CANTAT, I., MISBAH, C. & ZIMMERMANN, W. 2008 Lateral migration of a two-dimensional vesicle in unbounded Poiseuille flow. *Phys. Rev.* E **77**, 111702.

LEIGHTON, D. & ACRIVOS, A. 1987 The shear-induced migration of particles in concentrated suspensions. *J. Fluid Mech.* **181**, 415–439.

MAEDA, N., SUZUKI, Y., TANAKA, S. & TATEISHI, N. 1996 Erythrocyte flow and elasticity of microvessels evaluated by marginal cell-free layer and flow resistance. *Am. J. Physiol. Heart Circ. Physiol.* **271**, H2454–H2461.

MCWHIRTER, J. L., NOGUCHI, H. & GOMPPER, G. 2009 Flow-induced clustering and alignment of vesicles and red blood cells in microcapillaries. *Proc. Natl Acad. Sci. USA* **106**, 6039–6043.

OLLA, P. 1997 The role of tank-treading motions in the transverse migration of a spheroidal vesicle in a shear flow. *J. Phys.* A: *Math. Gen.* **30**, 317–329.

PAN, W. X., CASWELL, B. & KARNIADAKIS, G. E. 2010 A low-dimensional model for the red blood cell. *Soft Matt.* **6**, 4366–4376.

PIVKIN, I. V. & KARNIADAKIS, G. E. 2008 Accurate coarse-grained modeling of red blood cells. *Phys. Rev. Lett.* **101**, 118105.

POISEUILLE, J. L. M. 1835 Recherches sur les causes du mouvement du sang dans les vaisseaux capillaires. *C. R. Acad. Sci.* **6**, 554–560.

POISEUILLE, J. L. M. 1846 Recherches expérimentales sur le mouvement des liquides dans les tubes de très-petits diamêtres. *Mém. Preséntés par Divers Savants Acad. Sci. Inst. Fr.* **IX**, 433–544.

POZRIKIDIS, C. 2005 Numerical simulation of cell motion in tube flow. *Ann. Biomed. Engng* **33**, 165–178.

PRIES, A. R., NEUHAUS, D. & GAEHTGENS, P. 1992 Blood viscosity in tube flow: dependence on diameter and hematocrit. *Am. J. Physiol.* **263**, H1770–H1778.

PRIES, A. R. & SECOMB, T. W. 2008 Modeling structural adaptation of microcirculation. *Microcirculation* **15**, 753–764.

PRIES, A. R., SECOMB, T. W. & GAEHTGENS, P. 1996 Biophysical aspects of blood flow in the microvasculature. *Cardiovasc. Res.* **32**, 654–667.

PRIES, A. R., SECOMB, T. W. & GAEHTGENS, P. 2000 The endothelial surface layer. *Pflugers Arch.* **440**, 653–666.

PRIES, A. R., SECOMB, T. W., GESSNER, T., SPERANDIO, M. B., GROSS, J. F. & GAEHTGENS, P. 1994 Resistance to blood flow in microvessels in vivo. *Circulat. Res.* **75**, 904–915.

PRIES, A. R., SECOMB, T. W., SPERANDIO, M. & GAEHTGENS, P. 1998 Blood flow resistance during hemodilution: effect of plasma composition. *Cardiovasc. Res.* **37**, 225–235.

SECOMB, T. W. 1995 Mechanics of blood flow in the microcirculation. *Symp. Soc. Exp. Biol.* **49**, 305–321.

SECOMB, T. W. 2003 Mechanics of red blood cells and blood flow in narrow tubes. In *Hydrodynamics of Capsules and Cells* (ed. C. Pozrikidis), pp. 163–196. Chapman & Hall/CRC.

SECOMB, T. W. 2010 Mechanics and computational simulation of blood flow in microvessels. *Med. Engng Phys.*, **33**, 800–804.

SECOMB, T. W. & HSU, R. 1993 Non-axisymmetrical motion of rigid closely fitting particles in fluid-filled tubes. *J. Fluid Mech.* **257**, 403–420.

SECOMB, T. W., HSU, R. & PRIES, A. R. 1998 A model for red blood cell motion in glycocalyx-lined capillaries. *Am. J. Physiol.* **274**, H1016–H1022.

SECOMB, T. W., HSU, R. & PRIES, A. R. 2001 Effect of the endothelial surface layer on transmission of fluid shear stress to endothelial cells. *Biorheology* **38**, 143–150.

SECOMB, T. W., HSU, R. & PRIES, A. R. 2002 Blood flow and red blood cell deformation in nonuniform capillaries: effects of the endothelial surface layer. *Microcirculation* **9**, 189–196.

SECOMB, T. W. & SKALAK, R. 1982 A two-dimensional model for capillary flow of an asymmetric cell. *Microvasc. Res.* **24**, 194–203.

SECOMB, T. W., SKALAK, R., ÖZKAYA, N. & GROSS, J. F. 1986 Flow of axisymmetric red blood cells in narrow capillaries. *J. Fluid Mech.* **163**, 405–423.

SECOMB, T. W., STYP-REKOWSKA, B. & PRIES, A. R. 2007 Two-dimensional simulation of red blood cell deformation and lateral migration in microvessels. *Ann. Biomed. Engng* **35**, 755–765.

SEIFERT, U. 1999 Hydrodynamic lift on bound vesicles. *Phys. Rev. Lett.* **83**, 876–879.

SKOTHEIM, J. M. & MAHADEVAN, L. 2005 Soft lubrication: the elastohydrodynamics of nonconforming and conforming contacts. *Phys. Fluids* **17**, 092101.

SUKUMARAN, S. & SEIFERT, U. 2001 Influence of shear flow on vesicles near a wall: a numerical study. *Phys. Rev.* E **64**.

VAND, V. 1948 Viscosity of solutions and suspensions. I. Theory. *J. Phys. Colloid Chem.* **52**, 277–299.